

Supporting Information

Accelerating charge transfer for Ni(OH)₂ through chlorine-anion decoration in urea electrooxidation reaction

Yongjie Zhao,^a Xiujuan Sun,*^a Quhan Cao,^a Jiajia Zhou^a, Wenjuan Tan,^a Piao Zhu,^a Enhui Liu,^a Rui Ding,^a Ping Gao^a and Weiwei Lin,*^b

^a. Key Laboratory of Environmentally Friendly Chemistry and Applications of Ministry of Education, College of Chemistry, Xiangtan University, Hunan 411105, China.

^b. Anhui Laboratory of Functional Coordinated Complexes for Materials Chemistry and Application, Anhui Laboratory of Clean Catalytic Engineering, School of chemical and environmental Engineering, Anhui Polytechnic University, Wuhu, 241000, China.

Corresponding authors E-mails: sunxj594@xtu.edu.cn ; linweiwei@ahpu.edu.cn.

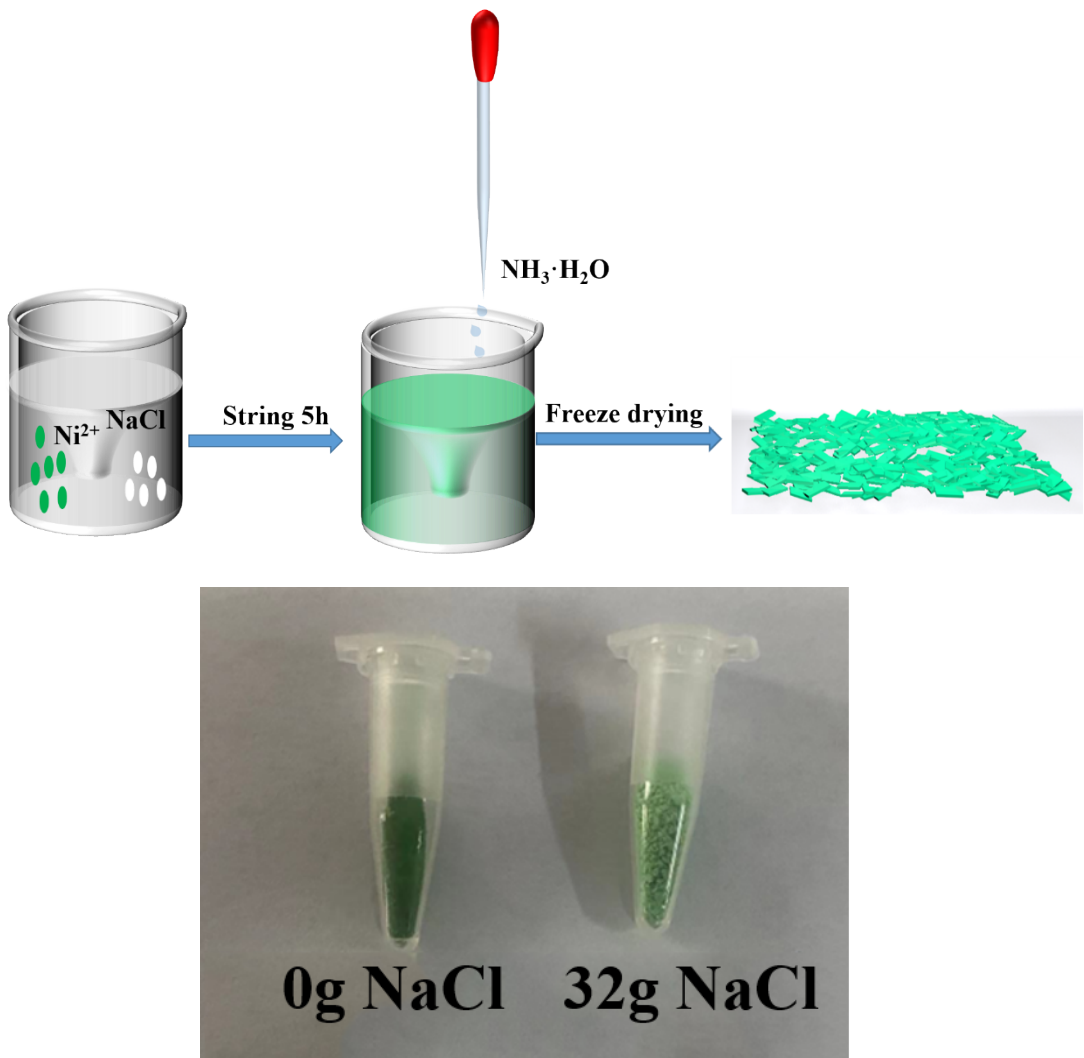


Fig. S1 Schematic diagram of the preparation process for the $\text{Cl}_{32}\text{-Ni(OH)}_2$ nanosheets and pictures of Ni(OH)_2 and $\text{Cl}_{32}\text{-Ni(OH)}_2$.

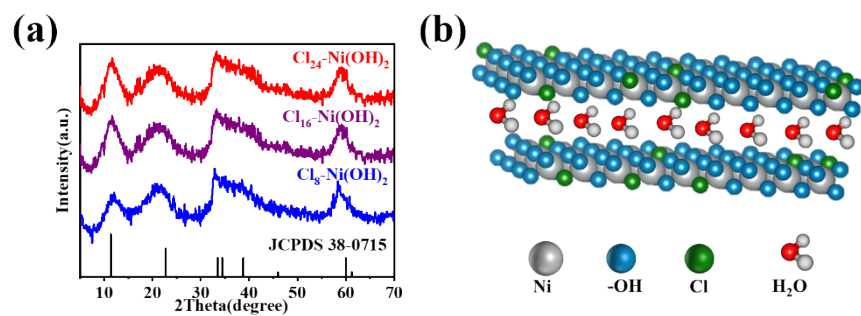


Fig. S2 (a)XRD patterns of $\text{Cl}_8\text{-Ni(OH)}_2$, $\text{Cl}_{16}\text{-Ni(OH)}_2$, $\text{Cl}_{24}\text{-Ni(OH)}_2$. (b) Cl- replaced partial OH- and the H_2O located between two Cl-Ni(OH)₂ layers

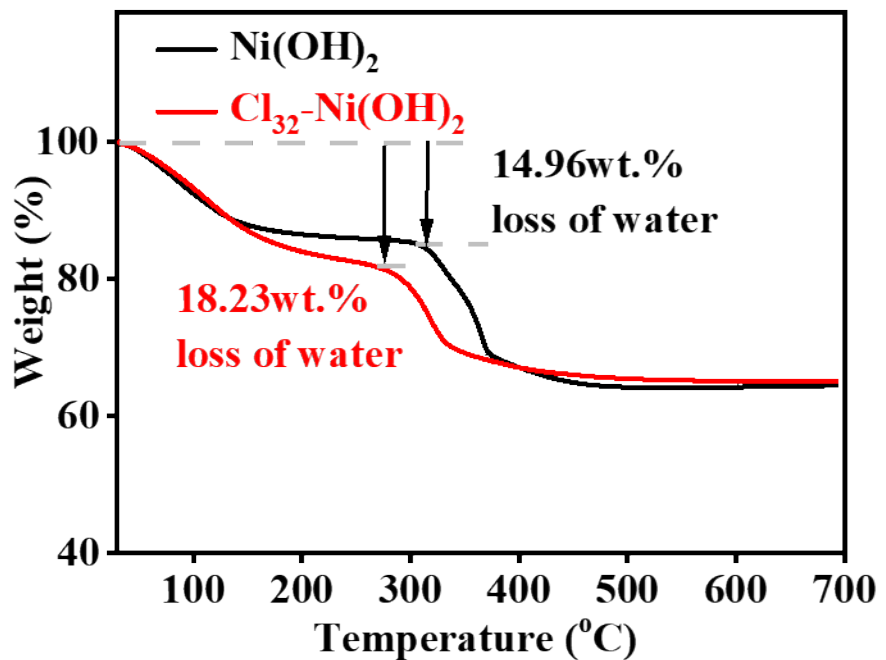


Fig. S3 Thermogravimetric curves of $\text{Ni}(\text{OH})_2$ and $\text{Cl}_{32}\text{-Ni}(\text{OH})_2$.

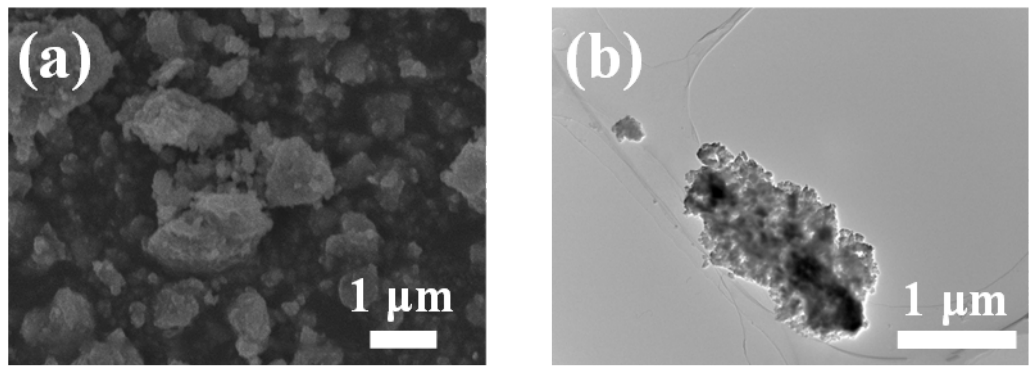


Fig. S4 (a) SEM and (b) TEM images of $\text{Ni}(\text{OH})_2$.

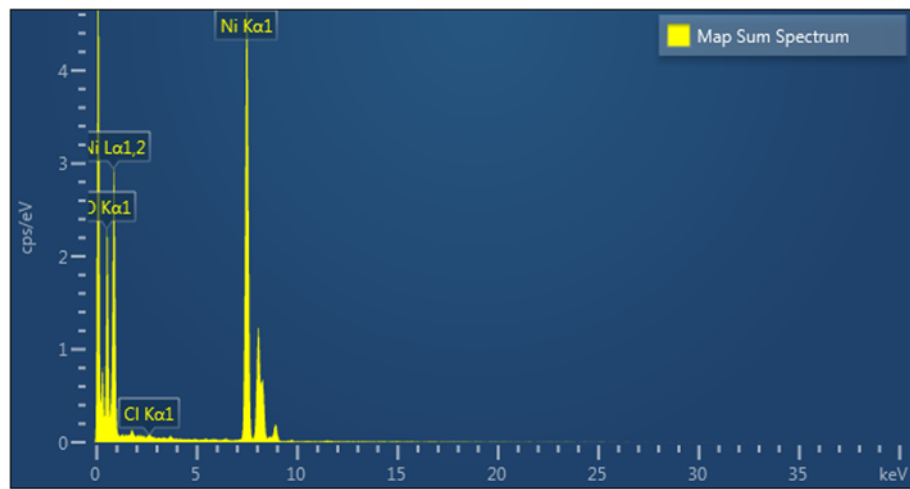


Fig. S5 EDX of Ni, O and Cl of $\text{Cl}_{32}\text{-Ni}(\text{OH})_2$.

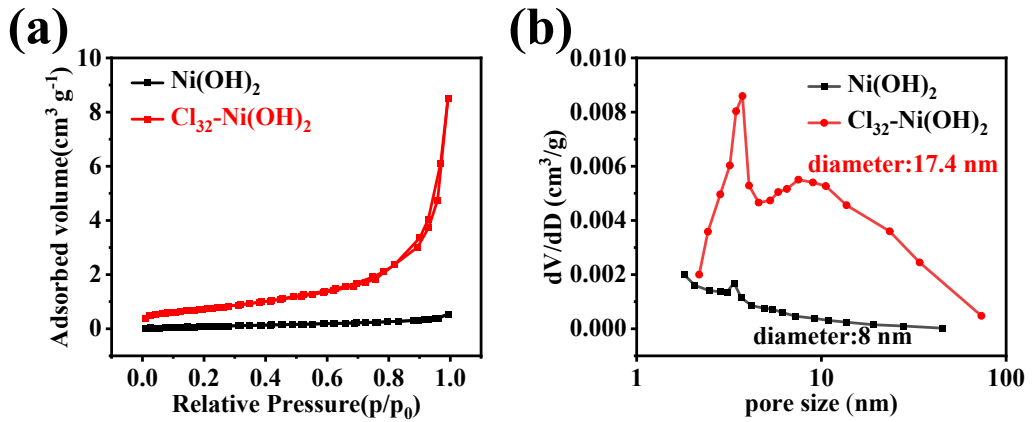


Fig. S6 a) N₂ adsorption-desorption isotherms and b) pore-size distributions of Ni(OH)₂ and Cl₃₂-Ni(OH)₂.

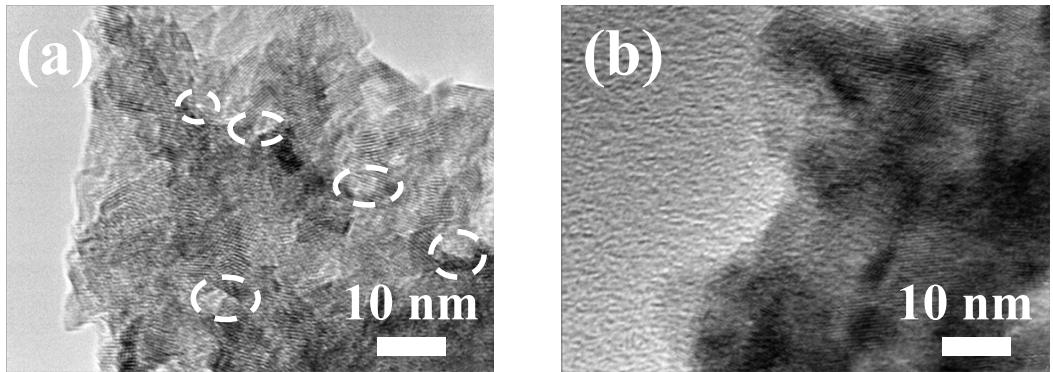


Fig. S7 HRTEM image of the (a) $\text{Cl}_{32}\text{-Ni}(\text{OH})_2$ and (b) $\text{Ni}(\text{OH})_2$.

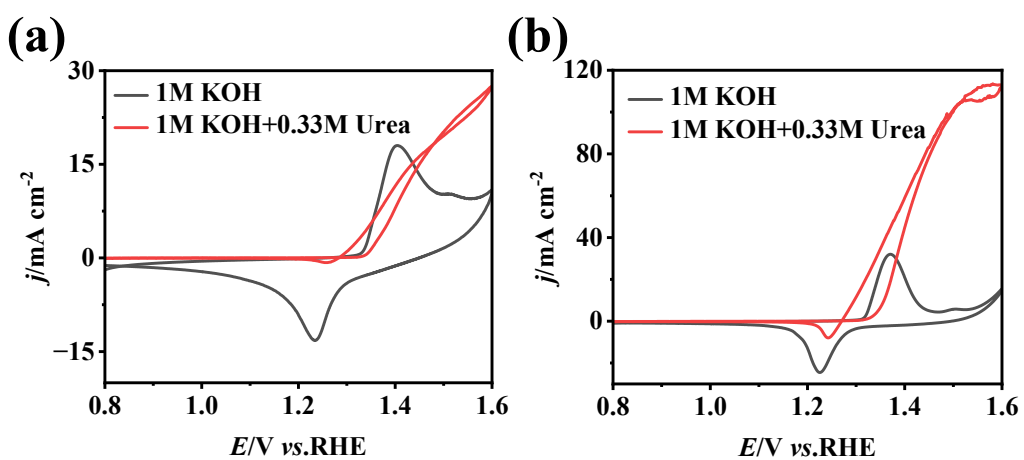


Fig. S8 Cyclic voltammograms of (a) Ni(OH)_2 and (b) $\text{Cl}_{32}\text{-Ni(OH)}_2$ electrocatalysts in 1.0 M KOH with/without 0.33 M urea solution.

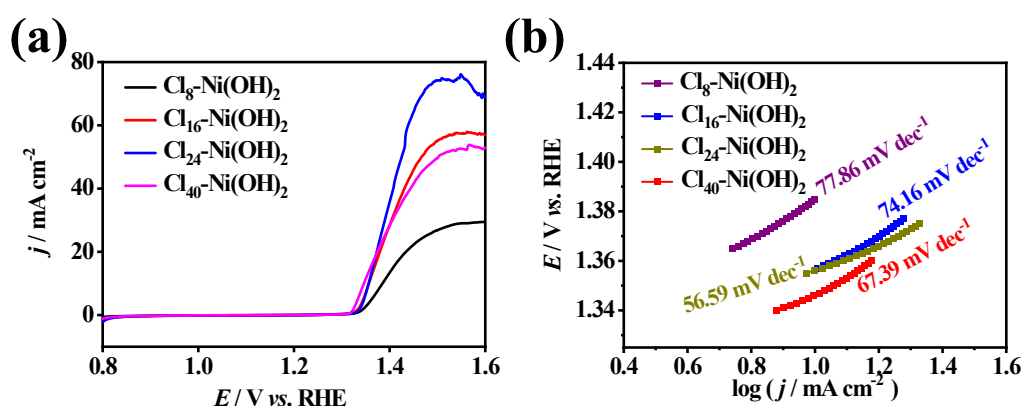


Fig. S9 The UOR performance of Ni(OH)_2 , $\text{Cl}_8\text{-Ni(OH)}_2$, $\text{Cl}_{16}\text{-Ni(OH)}_2$, $\text{Cl}_{24}\text{-Ni(OH)}_2$, $\text{Cl}_{40}\text{-Ni(OH)}_2$ (a) Polarization curves of different catalysts. (b) The Tafel slopes.

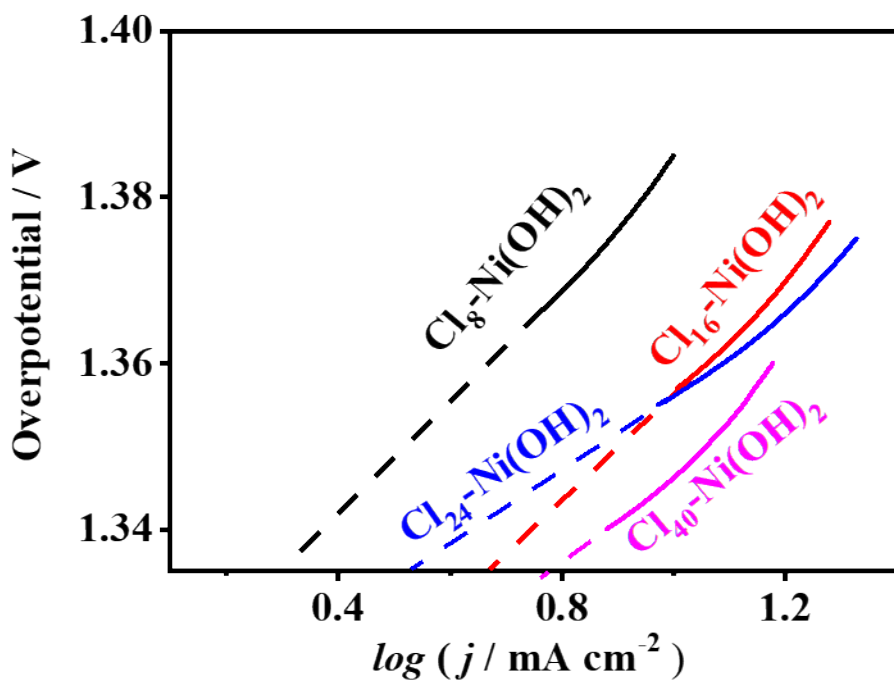


Fig. S10 Tafel plots of $\text{Cl}_8\text{-Ni(OH)}_2$, $\text{Cl}_{16}\text{-Ni(OH)}_2$, $\text{Cl}_{24}\text{-Ni(OH)}_2$ and $\text{Cl}_{40}\text{-Ni(OH)}_2$ to calculate the exchange current density.

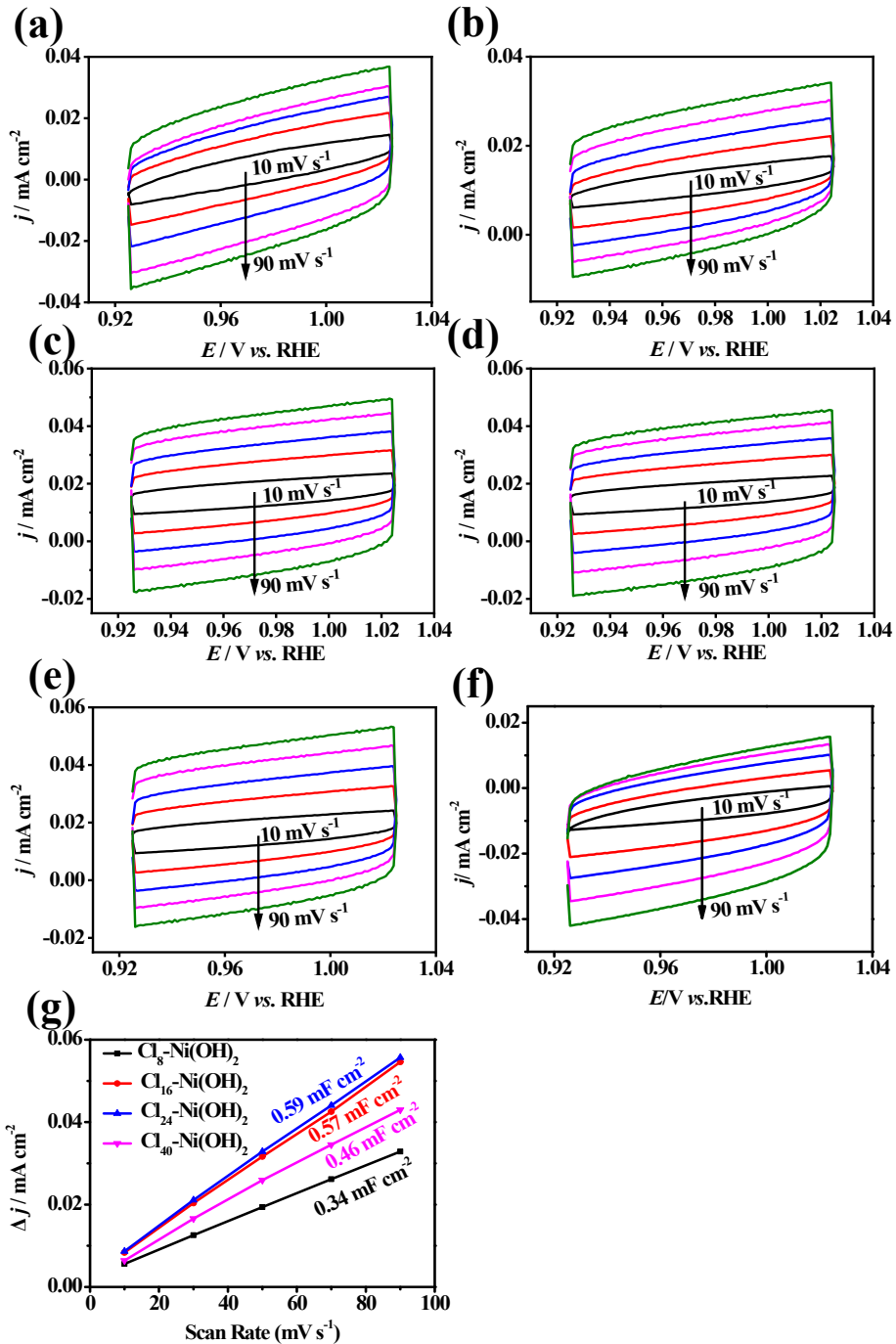


Fig. S11 Cyclic voltammograms (CV) of (a) Ni(OH)_2 , (b) $\text{Cl}_8\text{-Ni(OH)}_2$, (c) $\text{Cl}_{16}\text{-Ni(OH)}_2$, (d) $\text{Cl}_{24}\text{-Ni(OH)}_2$, (e) $\text{Cl}_{32}\text{-Ni(OH)}_2$, (f) $\text{Cl}_{40}\text{-Ni(OH)}_2$ at different scan rates of 10, 30, 50, 70, and 90 mV s^{-1} in 1 M KOH solution for C_{dl} testing at non-faradic reaction potential region for UOR. (g) The charging current density differences are plotted against the scan rates of the as-prepared catalysts. The linear slope is equivalent to twice of electrochemical double-layer capacitance (C_{dl}).

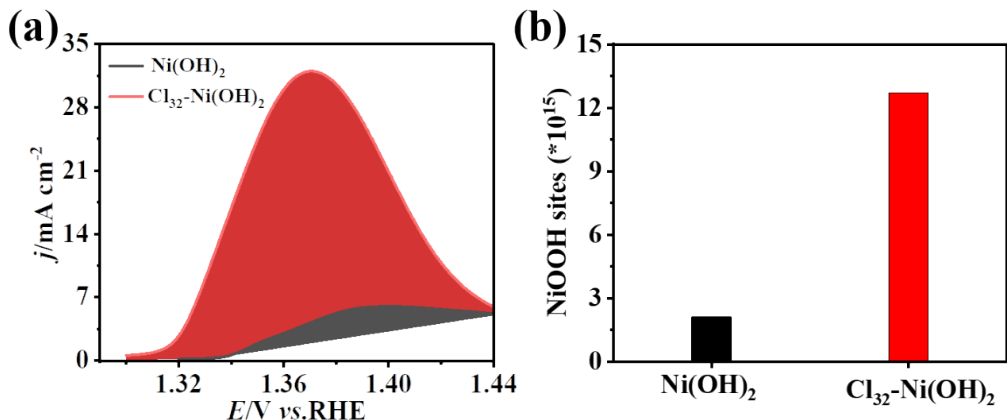


Fig. S12. (a) Oxidation peak areas, (b) The values of active sites

Due to the single-electron transfer process for the formation of NiOOH, the number of the active catalytic site can be derived from the area under the oxidation peak. The charge associated with the generated NiOOH is evaluated from Eq. (1).

$$\text{Charge associated with NiOOH formation} = \frac{\text{NiOOH peak area}}{\text{scan rate}}$$

The oxidation peak of $\text{Cl}_{32}\text{-Ni(OH)}_2$ shows a peak area of $2.04 \times 10^{-5} \text{ A V}$ with $2.04 \times 10^{-3} \text{ C}$ of charge associated with the NiOOH formation. Similarly, Ni(OH)_2 show $0.34 \times 10^{-3} \text{ C}$ of charge associated with single-electron oxidation of Ni^{2+} to NiOOH. The total number of active sites form on the electrocatalytic surface can be derived from the following Eq. (2).

$$N = \frac{\text{charge assosiated with oxidation peak}}{A \times \text{charge of electron}}$$

where N is the number of active sites, and A is the number of electrons transferred for the respective oxidation process.

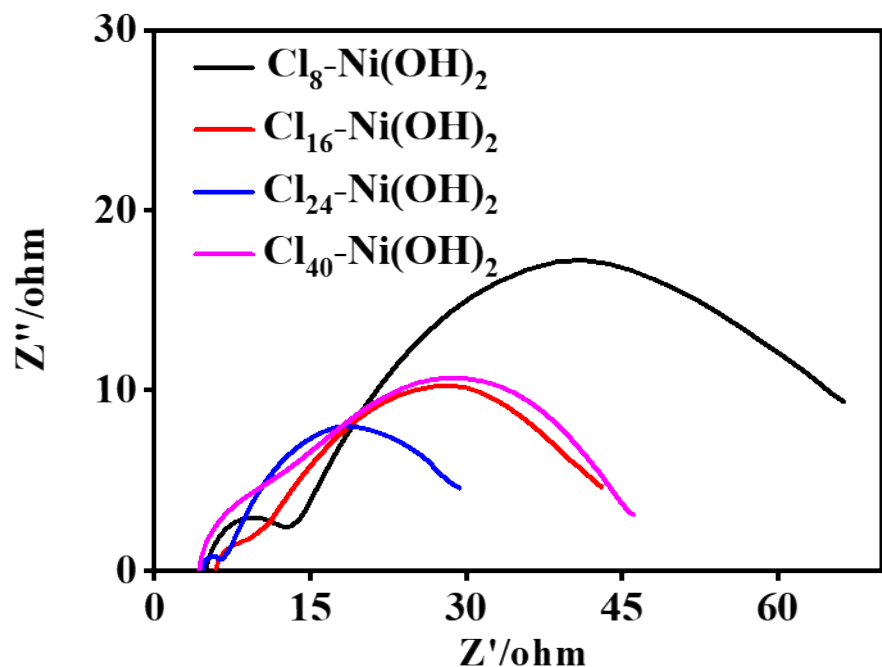


Fig. S13 Nyquist plots of the $\text{Cl}_8\text{-Ni(OH)}_2$, $\text{Cl}_{16}\text{-Ni(OH)}_2$, $\text{Cl}_{24}\text{-Ni(OH)}_2$, and $\text{Cl}_{40}\text{-Ni(OH)}_2$.

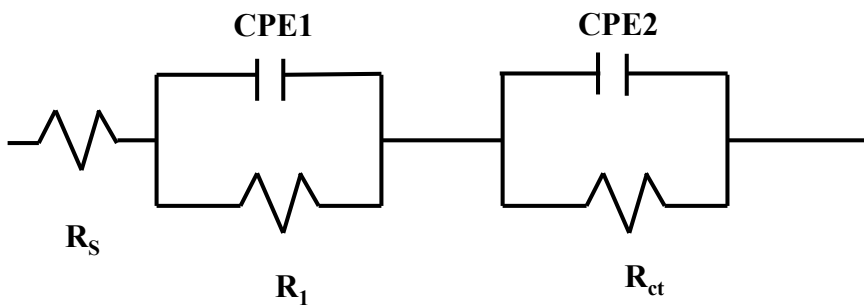


Fig. S14 The equivalent circuit model of EIS analysis.

The R_s is the uncompensated solution resistance. The R_{ct} at low frequency represents the charge transfer resistance and the value of R_1 at high frequency is denoted as the electrode surface contact resistance.

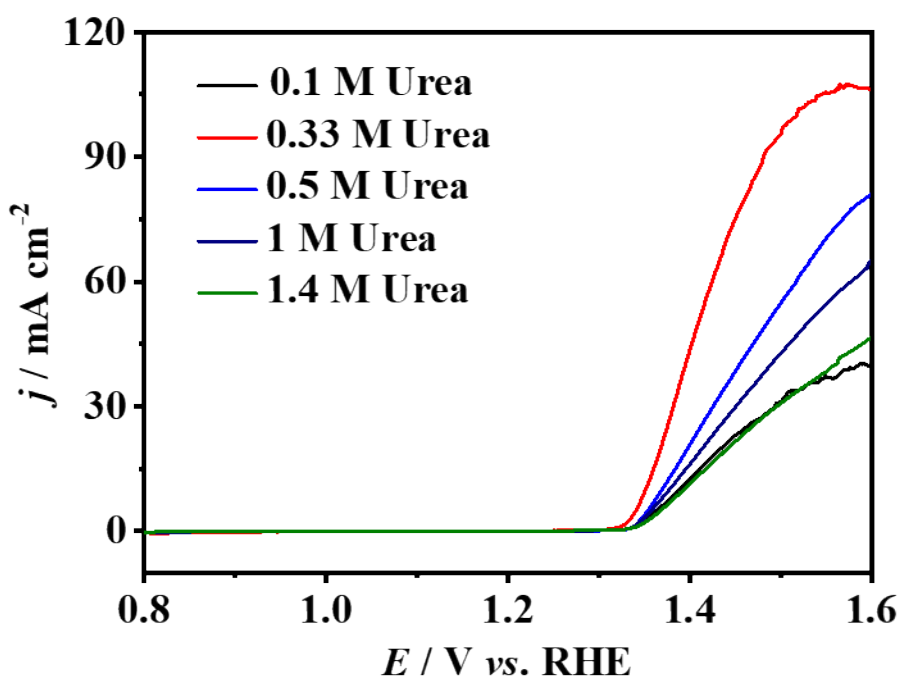


Fig. S15 The UOR performance of $\text{Cl}_{32}\text{-Ni(OH)}_2$ catalyst (a) in 1.0 M KOH with various urea concentrations.

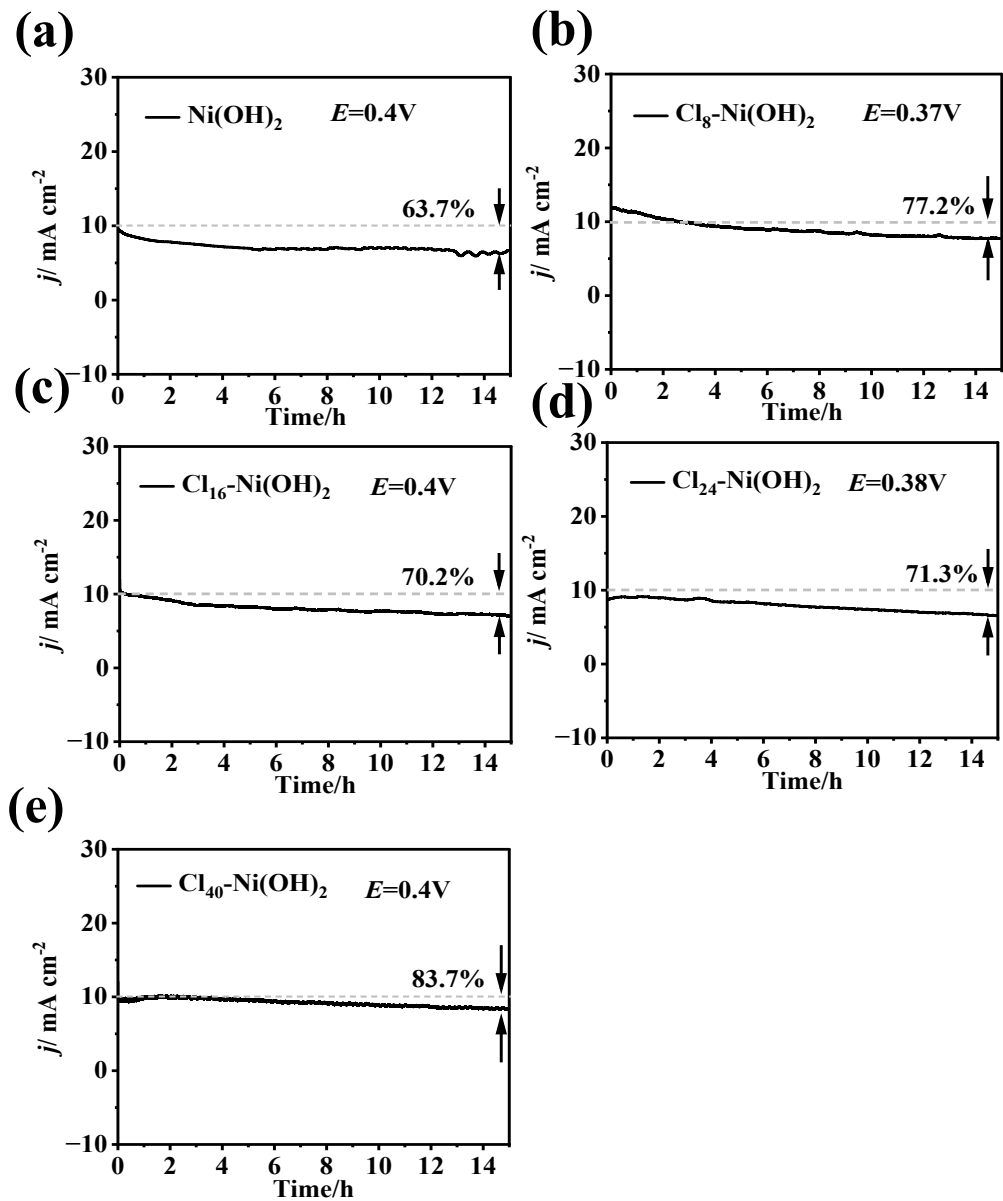


Fig. S16 Chronoamperometry test of Ni(OH)_2 , $\text{Cl}_8\text{-Ni(OH)}_2$, $\text{Cl}_{16}\text{-Ni(OH)}_2$, $\text{Cl}_{24}\text{-Ni(OH)}_2$ and $\text{Cl}_{40}\text{-Ni(OH)}_2$ measured for 15 h.

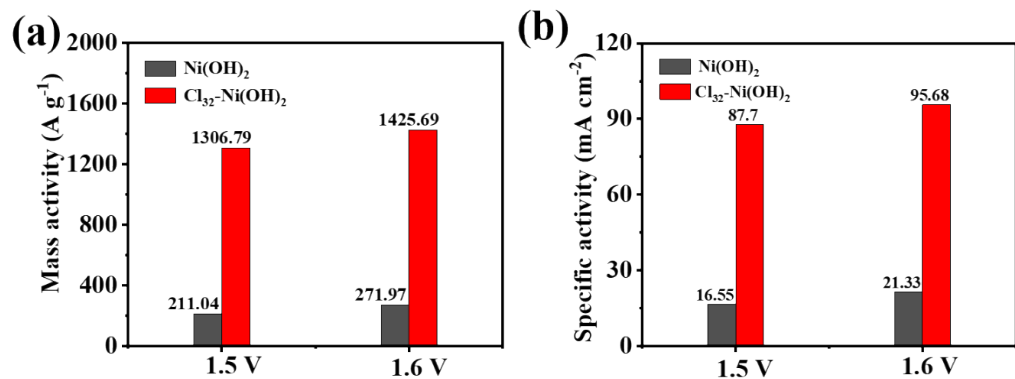


Fig.S17. The mass activities (a) and specific activities (b) of Cl₃₂-Ni(OH)₂ and Ni(OH)₂.

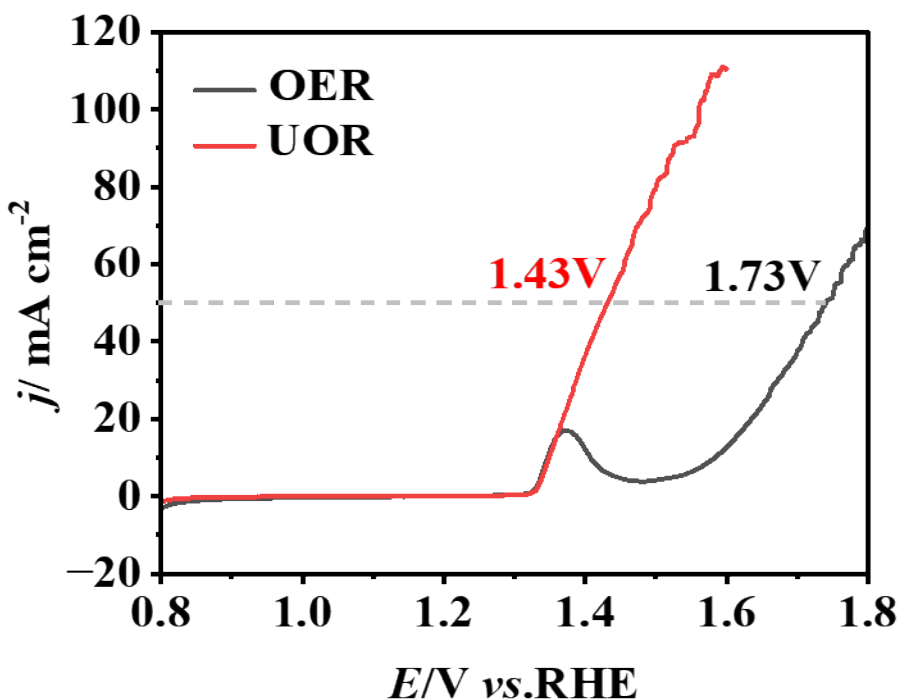


Fig. S18 Polarization curves for the UOR and OER of $\text{Cl}_{32}\text{-Ni}(\text{OH})_2$ electrode

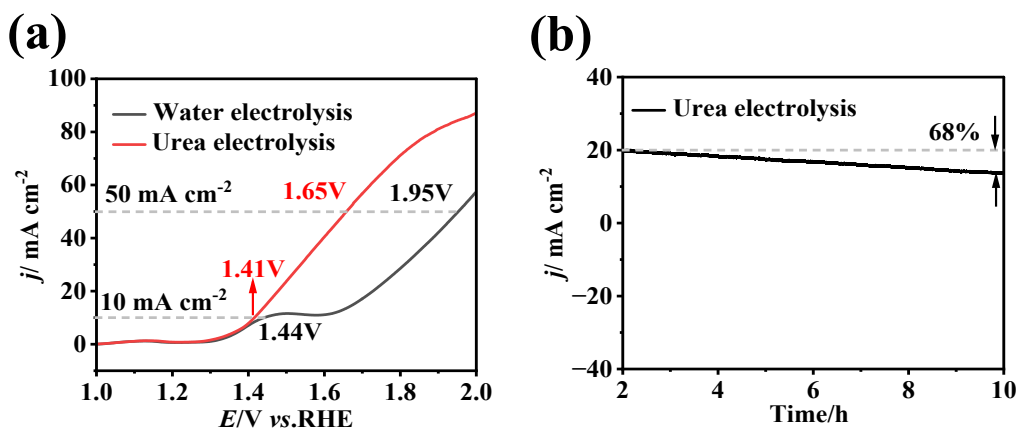


Fig. S19 (a) Comparison of polarization curves for the urea electrolysis and water electrolysis using $\text{Ni(OH)}_2/\text{CC}$ as the anode and the Pt/C/CC as the cathode.(b) The chronoamperometric curve of $\text{Cl}_{32}-\text{Ni(OH)}_2/\text{CC}$ in 1.0 M KOH with 0.33 M urea for 10 h

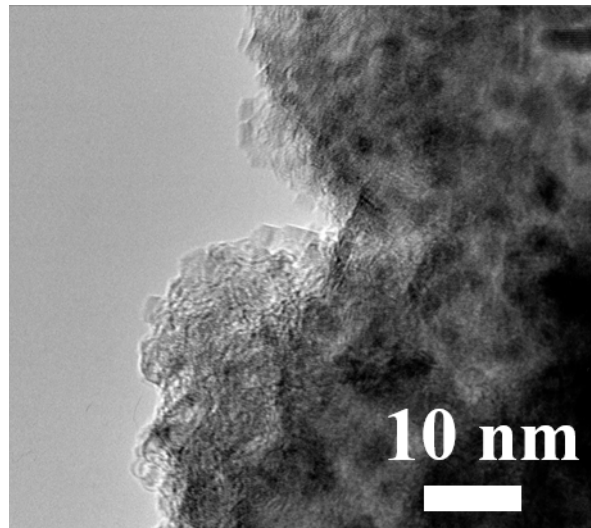


Fig. S20 HRTEM image of $\text{Cl}_{32}\text{-Ni}(\text{OH})_2$ after 15 h durability test.

Table S1. The XPS binding energies of Ni 2p, Cl 2p, O 1s for Ni(OH)₂, Cl₃₂-Ni(OH)₂.

Sample	Ni 2p	Cl 2p	O 1s
Ni(OH) ₂	855.6 eV, 873.0 eV (Ni ²⁺) 861.40 eV, 879.45 eV (sat.)	---	530.75eV (M-O) 531.49eV (O Vac) 532.47 eV (H-O-H)
Cl ₃₂ -Ni(OH) ₂	855.60 eV, 872.90 eV (Ni ²⁺) 857.80 eV, 874.90 eV (Ni ³⁺) 861.53 eV, 879.46 eV (sat.)	198.15 eV (Ni-Cl) 199.75 eV	530.50eV (M-O) 531.30eV (O_{Vac}) 532.90 eV (H-O-H)

Table S2. Comparison of the UOR performance of catalysts reported in the literature.

Catalysts	Electrolyte	Potential (V vs.RHE)	Current density (mA cm ⁻²)	Substrate	Ref.
Cl₃₂-Ni(OH)₂	1 M KOH + 0.33 M urea	1.6	106.15	GC	This work
Ni ₆₀ Cr ₄₀ /C	1 M KOH + 0.33 M urea	1.6	~90	GC	1
Ni MOF (BTC)	1 M KOH + 0.33 M urea	1.6	~89	GC	2
Ni-Co	1 M KOH + 0.33 M urea	1.6	~21	GC	3
Ni(OH) ₂ /PPy/ GO	1 M KOH + 0.5 M urea	1.6	~13	GC	4
Metallic Ni(OH) ₂	1 M KOH + 0.33 M urea	1.52	~35	GC	5
NiMn/C	1 M KOH + 0.33 M urea	1.6	~42	GC	6
Ni/Sn dendrites	1 M KOH + 0.33 M urea	1.55	~44	GC	7
Ni-MOF @NiO/Ni-2	1 M KOH + 0.33 M urea	1.6	~80	GC	8
Ni ₂ P	1 M KOH + 0.5 M urea	1.6	~90	GC	9
Ni(OH) ₂ nanomeshes1	1 M KOH + 0.33 M urea	1.6	~45	GC	10
NiCo alloys	1 M KOH + 0.3 M urea	1.6	~32	GC	11

Table S3. Impedance parameter values obtained from the fitting to the equivalent circuit for the Nyquist plots in 1.0 M KOH and 0.33 M urea. The R_s , R_1 and R_{ct} correspond to the solution resistance, oxide film resistance and charge-transfer resistance, respectively.

Sample	R_s	R_1	R_{ct}
Ni(OH) ₂	4.643	33.32	193.3
Cl ₈ -Ni(OH) ₂	4.932	7.878	56.09
Cl ₁₆ -Ni(OH) ₂	5.802	3.971	35.38
Cl ₂₄ -Ni(OH) ₂	4.618	1.967	25.13
Cl₃₂-Ni(OH)₂	4.297	2.688	16.39
Cl ₄₀ -Ni(OH) ₂	4.228	5.702	37.67

Table S4. Comparison of the overall urea electrolysis performance of as-prepared Pt/C/CC||Cl₃₂-Ni(OH)₂/CC and recently reported active catalysts.

Samples	Electrolytes (1 M KOH)	Voltage (V@10 mA cm ⁻² vs. RHE)	Ref.
Cl₃₂-Ni(OH)₂/CC Pt/C/CC	+0.33 M Urea	1.38	This work
NiFe/N-C Pt	+1 M Urea	1.50	12
Ni _x Co _{2-x} P/C@HCNs/CC	+0.33 M Urea	1.47	13
Co ₃ Mo ₁ S-CC Co ₃ Mo ₁ S-CC	+0.5 M Urea	1.50	14
Ni/C Ni/C	+0.33 M Urea	1.60	15
Ni-MOF-0.5 Ni-MOF-0.5	+0.5 M Urea	1.52	16
CoFeCr LDH/NF Pt-C/NF	+0.33 M Urea	1.329	17
Fe _{11.1%} -Ni ₃ S ₂ /NF	+ 0.33 M urea	1.46	18
Ni ₂ P/Fe ₂ P/NF	+ 0.5 M urea	1.47	19
Ni-MOF@NiO/Ni/NF Pt-C/NF	+ 0.33 M urea	1.42	8

References

1. R. K. Singh and A. Schechter, *Chemcatchem*, 2017, **9**, 3374-3379.
2. V. Maruthapandian, S. Kumaraguru, S. Mohan, V. Saraswathy and S. Muralidharan, *Chemelectrochem*, 2018, **5**, 2795-2807.
3. W. Xu, H. M. Zhang, G. Li and Z. C. Wu, *Sci Rep-Uk*, 2014, **4**, 5863.
4. Z. Q. Cao, H. Mao, X. Guo, D. Y. Sun, Z. J. Sun, B. X. Wang, Y. Zhang and X. M. Song, *Acs Sustain Chem Eng*, 2018, **6**, 15570-15581.
5. X. J. Zhu, X. Y. Dou, J. Dai, X. D. An, Y. Q. Guo, L. D. Zhang, S. Tao, J. Y. Zhao, W. S. Chu, X. C. Zeng, C. Z. Wu and Y. Xie, *Angew Chem Int Edit*, 2016, **55**, 12465-12469.
6. N. A. M. Barakat, M. Alajami, Z. K. Ghouri and S. Al-Meer, *Nanomaterials-Basel*, 2018, **8**, 338.
7. R. K. Singh, P. Subramanian and A. Schechter, *Chemelectrochem*, 2017, **4**, 1037-1043.
8. Q. Li, S. S. Zheng, M. Du and H. Pang, *Chem Eng J*, 2021, **417**, 129201.
9. H. P. Liu, S. L. Zhu, Z. D. Cui, Z. Y. Li, S. L. Wu and Y. Q. Liang, *Nanoscale*, 2021, **13**, 1759-1769.
10. Y. Ding, Y. Li, Y. Y. Xue, B. Q. Miao, S. N. Li, Y. C. Jiang, X. Liu and Y. Chen, *Nanoscale*, 2019, **11**, 1058-1064.
11. W. Huang, K. L. Wang, Q. H. Cao, Y. J. Zhao, X. J. Sun, R. Ding, E. H. Liu, P. Gao and G. J. Li, *New J Chem*, 2021, **45**, 2943-2947.
12. J. Zhang, F. Xing, H. Zhang and Y. Huang, *Dalton Transactions*, 2020, **49**, 13962-13969.
13. S. Rezaee and S. Shahrokhan, *Nanoscale*, 2020, **12**, 16123-16135.
14. P. Li, Z. Zhuang, C. Du, D. Xiang, F. Zheng, Z. Zhang, Z. Fang, J. Guo, S. Zhu and W. Chen, *ACS Applied Materials & Interfaces*, 2020, **12**, 40194-40203.
15. L. Wang, L. Ren, X. Wang, X. Feng, J. Zhou and B. Wang, *ACS Applied Materials & Interfaces*, 2018, **10**, 4750-4756.
16. S. Zheng, Y. Zheng, H. Xue and H. Pang, *Chemical Engineering Journal*, 2020, **395**, 125166.
17. Z. Wang, W. Liu, Y. Hu, M. Guan, L. Xu, H. Li, J. Bao and H. Li, *Applied Catalysis B: Environmental*, 2020, **272**, 118959.
18. W. Zhu, Z. Yue, W. Zhang, N. Hu, Z. Luo, M. Ren, Z. Xu, Z. Wei, Y. Suo and J. Wang, *Journal of Materials Chemistry A*, 2018, **6**, 4346-4353.
19. L. Yan, Y. Sun, E. Hu, J. Ning, Y. Zhong, Z. Zhang and Y. Hu, *Journal of colloid and interface science*, 2019, **541**, 279-286.